



in 0.5 ml of FCS. These preparations were examined with a fluorescence microscope (Leitz) and photographed with a Nikon FE camera. The remainder of each sample was used for cell sorting in a fluorescence-activated cell sorter (FACS III; Becton Dickinson) with a 70- $\mu$ m nozzle. The laser settings were at their lowest level. Table 1 shows the data from triplicate cell-sorting studies with myocytes, liver cells not containing myosin, and murine myeloma (NS-1) cells cultured in glucose-free or high-glucose medium under an N<sub>2</sub> or a normal O<sub>2</sub> atmosphere. Control Co-AA-labeled myocytes grown in high-glucose medium under normal O<sub>2</sub> atmosphere showed mainly nonspecific adsorption of beads (0 to 5). When myocytes were grown under identical conditions but exposed to Co-AM spheres, the presence of damaged myocytes that had adsorbed more than 25 beads per cell became apparent, as well as a population of either minimally compromised or intact myocytes that had adsorbed only 0 to 5 beads. The ratio of high to low fluorescence events was employed as an indicator of injury, showing maximum damage in cells grown in glucose-free medium under N<sub>2</sub> atmosphere and minimal damage in high-glucose medium under normal O<sub>2</sub> atmosphere. Furthermore, these ratios of fluorescence are significantly different from those found in the myocytes exposed to Co-AA, which was employed as a measure of nonspecific labeling ( $P < .001$ ). Mouse liver cells and mouse myeloma cells (NS-1) in high-glucose medium under N<sub>2</sub> atmosphere were also used as non-myosin-containing cell controls. These control cells showed similar nonspecific adsorption of both Co-AMM and Co-AA (Table 1;  $P$ , not significant). A set of culture flasks treated similarly was subjected to scanning electron microscopy (8).

Myocytes bearing Co-AMM, grown in glucose-free DMEM-FCS, are shown in Fig. 1. When cells were grown in high-glucose DMEM-FCS, the results were similar to those obtained in cells grown in the glucose-free medium, but fewer dead cells were seen. The fluorescence micrographs of dead myocytes stained with Co-AMM and the corresponding light micrograph are shown in Fig. 1, a and b. The control fluorescence micrograph with Co-AA showing only minimal binding of fluorescent microspheres (Fig. 1c) and its corresponding light micrograph (Fig. 1d) are also shown.

Necrotic myocytes still retained their cell shape even after trypsin dissociation, although integrity of the cell membrane was lost. The scanning electron

microscope was used to locate the site of binding of the microspheres coated with antibody specific for myosin. Electron micrographs show an intact myocyte (Fig. 2a) with very few adherent spheres and necrotic myocytes (Fig. 2b) with a dense accumulation of Co-AMM over a hole in the cell membrane through which intracellular contents appear to be herniating. The binding of Co-AMM to cardiac myofibrils exposed through a hole in the membrane of a necrotic myocyte is shown at much higher magnification in Fig. 2c.

The substantial adsorption of Co-AMM to necrotic myocytes was readily differentiated from the lesser, nonspecific adsorption of Co-AA by the FACS III. Figure 3 shows FACS III dot-plot analy-

ses (where the abscissa is cell size; the ordinate, intensity of fluorescence; and each point, a fluorescence event) of control Co-AA adsorption to dead myocytes in high-glucose DMEM-FCS (a) and specific adsorption of Co-AMM to dead myocytes in high-glucose DMEM-FCS (b). Similar results were also obtained with myocytes grown in glucose-free DMEM under an N<sub>2</sub> atmosphere—an intervention aimed at promoting cell death by simulating an ischemic environment. Fluorescence intensity was least when the nonspecific antibody-labeled spheres (Co-AA) were employed, increased when specific antibody-labeled spheres (Co-AMM) were exposed to cells treated in high-glucose medium, and was most marked when the specific

Table 1. Effects of glucose-free medium and N<sub>2</sub> on cell staining. Approximately 10<sup>4</sup> cells were sorted in each group. High (H) indicates > 25 beads and low (L), 0 to 5 beads. Abbreviation: N.M.F., no measurable fluorescence detected.

Medium	Labeled Covasphere	Fluorescence events ( $\times 10^{-3}$ )		H/L	Fluorescence events/total cells sorted
		High	Low		
<i>Myocytes</i>					
Glucose-free	Co-AMM	1.5 $\pm$ 0.2	4.0 $\pm$ 0.1	0.40*	0.52
Glucose-free + N <sub>2</sub>	Co-AMM	4.0 $\pm$ 0.4	3.4 $\pm$ 0.4	1.2*†	0.57
High-glucose	Co-AMM	1.6 $\pm$ 0.3	5.1 $\pm$ 0.8	0.29*	0.51
High-glucose + N <sub>2</sub>	Co-AMM	1.6 $\pm$ 0	2.57 $\pm$ 0.4	0.63*†	0.55
High-glucose	Co-AA	N.M.F.	1.7 $\pm$ 0.2	0.0	0.40
<i>Liver cells</i>					
High-glucose + N <sub>2</sub>	Co-AMM	0.3 $\pm$ 0.3	3.8 $\pm$ 0.5	0.08	0.41
High-glucose + N <sub>2</sub>	Co-AA	0.2 $\pm$ 0	4.05 $\pm$ 0.5	0.10	0.43
<i>NS-1</i>					
High-glucose + N <sub>2</sub>	Co-AMM	0.1 $\pm$ 0.05	3.2 $\pm$ 0.3	0.03	0.33
High-glucose + N <sub>2</sub>	Co-AA	0.1 $\pm$ 0	3.1 $\pm$ 0.05	0.03	0.32

\* $P < .001$  when compared to H/L of cells exposed to Co-AA in high-glucose medium; values denote mean  $\pm$  standard deviation. † $P < .001$  when compared to cells exposed to Co-AMM in high-glucose medium.

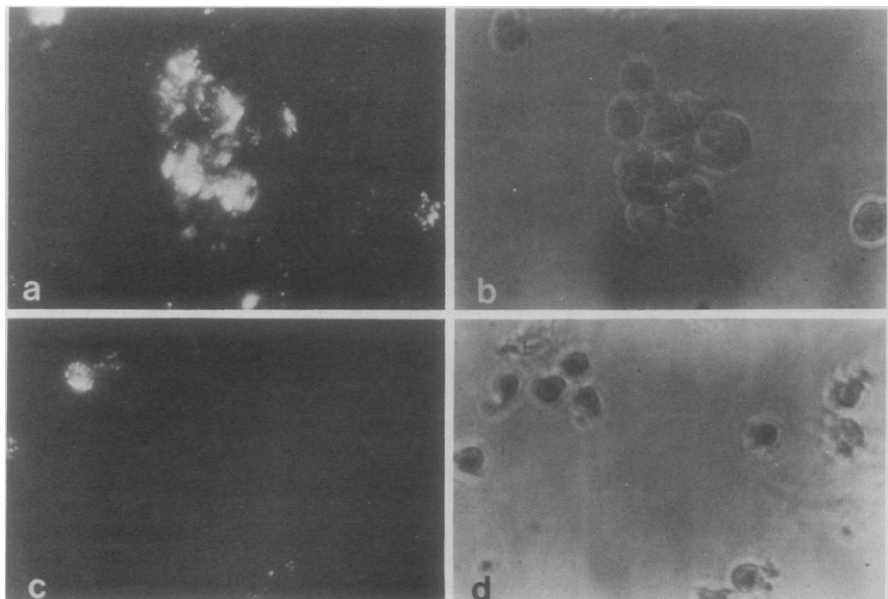


Fig. 1. (a) Fluorescence micrograph demonstrating localization of Co-AMM in necrotic myocytes in glucose-free culture medium; (b) corresponding light micrograph ( $\times 252$ ). (c) Fluorescence micrograph of nonspecific adsorption of control Co-AA by cultured myocytes in glucose-free medium; (d) corresponding light micrograph.

antibody-labeled spheres (Co-AMM) were mixed with cells incubated in glucose-free medium under an N<sub>2</sub> atmosphere. It is apparent from the quantitative analyses (Fig. 3, a and b) that necrotic cells were present even in the high-glucose medium, but they were consistently fewer in number. Glucose deprivation alone produced a small increase in the high-fluorescence cell population, although a significant increase in cell death was not affected ( $P < .1$ ), a finding previously observed by Acosta *et al.* (9). The ratio of high to low fluorescence events increased approximately fourfold in the glucose-free medium un-

der an N<sub>2</sub> atmosphere (Table 1). Thus it appears that Co-AMM can specifically discriminate necrotic from live myocytes and that nonspecific adsorption of spheres coated with another, irrelevant antibody is minimal. Identification of dead cells is based on the number of Co-AMM bound to the cell surface. Cells bearing more than 25 beads (Fig. 3, c and d) could be readily separated from cells bearing 0 to 5 beads, the latter representing nonspecific adsorption, in that a similar degree of binding was seen with Co-AA spheres. The cells were sorted at a rate of 200 to 400 cells per second, and physical separation of live from dead

cells was readily effected. Cells that were heavily labeled (>20 beads) were nonviable and did not survive in culture. In contrast, those that carried only a few microspheres continued to contract and grow in culture after their retrieval from the cell sorter. These cells, although viable, may constitute a population of compromised myocytes that can easily be separated from irreversibly damaged necrotic cells.

This study indicates that antibodies specific for cardiac myosin can discriminate live from dead myocytes with considerable specificity; it also provides a unique method for measuring and describing those elements critical in determining cell viability. Thus the process of cell injury may be viewed during its evolution, and pure populations of cells could be separated on the basis of viability at any time, so that detailed biochemical analyses of membrane integrity or intracellular processes, such as high-energy phosphate depletion, can be measured. Antibody specific for myosin should be capable of detecting the early disruption of membrane integrity, although the sensitivity of this technique requires further definition. This indicator of cell injury can then be compared with other methods, such as supravital staining with nuclear dyes (for example, propidium iodide) or with biochemical indices of necrosis. Finally, the method allows exact quantitation of cell death, and, therefore, the efficacy of interventions aimed at salvaging ischemic myocardial cells can be judged in a rigorous fashion.

B. A. KHAW

Cardiac Unit, Massachusetts General Hospital, and Harvard Medical School, Boston 02114

J. SCOTT

Department of Radiology, Massachusetts General Hospital, and Harvard Medical School

J. T. FALLON

Department of Pathology, Massachusetts General Hospital, and Harvard Medical School

S. L. CAHILL

E. HABER

C. HOMCY\*

Cardiac Unit, Massachusetts General Hospital, and Harvard Medical School

#### References and Notes

1. W. E. Shell, J. K. Kjekshus, B. E. Shell, *J. Clin. Invest.* **50**, 2514 (1971); I. Mydick, F. Wroblewski, J. S. La Due, *Circulation* **12**, 161 (1955); B. E. Sobel and W. E. Shell, *ibid.* **45**, 471 (1972).
2. B. A. Khaw, G. A. Beller, E. Haber, T. W. Smith, *J. Clin. Invest.* **58**, 439 (1976); J. T. Willerson, P. Kulkarni, M. Stone, S. E. Lewis, E. Eigenbrodt, F. Bonte, R. W. Parkey, L. M. Buja, *Proc. Natl. Acad. Sci. U.S.A.* **77**, 6856 (1980).

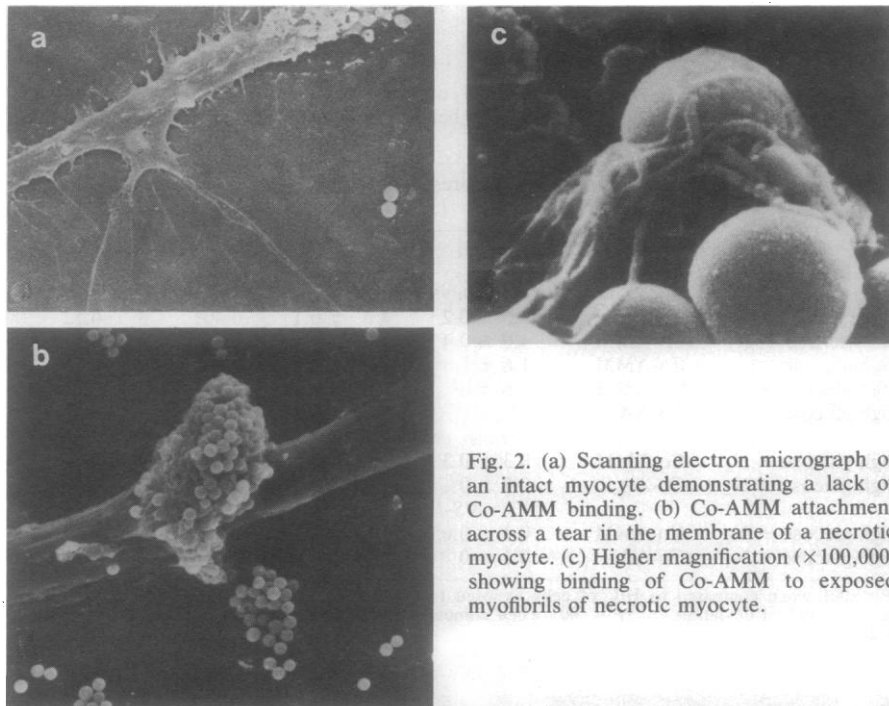


Fig. 2. (a) Scanning electron micrograph of an intact myocyte demonstrating a lack of Co-AMM binding. (b) Co-AMM attachment across a tear in the membrane of a necrotic myocyte. (c) Higher magnification ( $\times 100,000$ ) showing binding of Co-AMM to exposed myofibrils of necrotic myocyte.

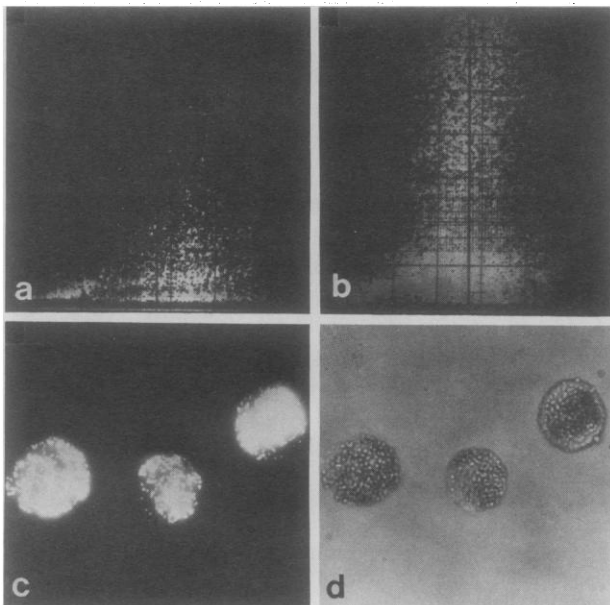


Fig. 3. (a) and (b) The dot-plot analyses (abscissa, cell size; ordinate, fluorescence intensity; each point is a fluorescence event) obtained on the fluorescence-activated cell sorter utilizing Co-AA (frame a) in a high-glucose medium, demonstrating a minimal amount of nonspecific adsorption. In contrast, the corresponding dot plots using specific Co-AMM (frame b) show marked fluorescence of necrotic myocytes ( $10^5$  cells were analyzed). (c) A fluorescence micrograph of sorted necrotic myocytes with a large number of bound Co-AMM and (d) the corresponding light micrograph.

3. B. A. Khaw, G. A. Beller, E. Haber, *Circulation* 57, 743 (1978); B. A. Khaw, H. K. Gold, R. Leinbach, J. T. Fallon, W. Strauss, G. M. Pohost, E. Haber, *ibid.* 58, 1137 (1978).
  4. B. A. Khaw, J. T. Fallon, G. A. Beller, E. Haber, *ibid.* 60, 1527 (1979); B. A. Khaw, J. T. Fallon, H. W. Strauss, E. Haber, *Science* 209, 295 (1980).
  5. A. M. Katz, I. Doris, C. T. Repke, B. B. Rubin, *Circ. Res.* 19, 611 (1965).
  6. Covaspheres were purchased from Covalent Technology Corporation, San Jose, Calif.
  7. J. A. Scott, C. D. Leder, S. W. Miller, G. M. Kolodny, *Invest. Radiol.* 16, 141 (1981).
  8. Cells submitted for scanning electron microscopy were fixed in their culture dishes after brief washing and addition of 5 ml of cacodylate-buffered 2 percent glutaraldehyde-paraformaldehyde for 2 hours. The cells were postfixed in 1 percent osmium for 1 hour, rinsed in buffer, and while in buffer the culture dishes containing the cells were cut into square pieces 1 by 1 cm. Four to five pieces from each culture dish were dehydrated in ethyl alcohol, critical point-dried, sputter-coated with 200 Å of gold-palladium, and examined in an AMR-1400 scanning electron microscope.
  9. D. Acosta, M. Puckett, R. McMillin, *In Vitro* 14, 728 (1978).
  10. Supported in part by PHS grant HL-17665, American Heart Association Established Investigatorship 80-148 (C.H.), and a grant from R. J. Reynolds Industries. We thank R. Rubin for editorial assistance.
- \* Address reprint requests to Dr. Charles J. Homcy, Cellular and Molecular Research Laboratory, Massachusetts General Hospital, Boston 02114.

1 March 1982; revised 4 May 1982

## Intraneuronal Aluminum Accumulation in Amyotrophic Lateral Sclerosis and Parkinsonism-Dementia of Guam

**Abstract.** *Scanning electron microscopy with energy-dispersive x-ray spectrometry was used to analyze the elemental content of neurofibrillary tangle (NFT)-bearing and NFT-free neurons within the Sommer's sector (H<sub>1</sub> region) of the hippocampus in Guamanian Chamorros with amyotrophic lateral sclerosis and parkinsonism-dementia and in neurologically normal controls. Preliminary data indicate prominent accumulation of aluminum within the nuclear region and perikaryal cytoplasm of NFT-bearing hippocampal neurons, regardless of the underlying neurological diagnosis. These findings further extend the association between intraneuronal aluminum and NFT formation and support the hypothesis that environmental factors are related to the neurodegenerative changes seen in the Chamorro population.*

The indigenous (Chamorro) population of Guam represents one of three geographical foci in the western Pacific region where inordinately high incidence rates of amyotrophic lateral sclerosis (ALS) and parkinsonism in association with severe dementia (parkinsonism-dementia or PD) are found (1). Severe neurofibrillary tangle (NFT) formation has been demonstrated in central nervous system tissues from affected patients (2) and from a high proportion of neurologically intact individuals of a relatively young age (3). Comparatively high levels of aluminum and unusually low levels of calcium and magnesium have been found in samples of drinking water and garden soils from Guam and two other high incidence foci of ALS and PD, one in the Kii Peninsula of Japan (4) and the other in southern West New Guinea (5, 6). Accordingly, we have, following Yase's suggestions (7), suspected that chronic nutritional deficiencies of calcium and magnesium and relative excesses of certain nonessential trace metals (such as aluminum) may produce aberrations in mineral metabolism, resulting in abnormal deposition of these elements in the central nervous system.

Brain tissues from eight Guamanian Chamorros (one ALS, two PD, and five neurologically normal controls), who were lifelong residents of the island,

were examined. The clinical courses of the two PD cases (ages, 57 and 66 years) and the ALS case (age, 64 years) were typical and the neuropathological changes were confirmatory. The five control cases were Chamorros who died of nonneurological disorders, and, although they had not been subjected to careful neurological evaluation, they were considered to be free of any significant neurological dysfunction. Neuropathologically, none of the controls had evidence of extrapyramidal or motor neuron degeneration. On the basis of silver impregnation staining, four of the control cases (ages, 48, 48, 57, and 65

years) had no NFT-bearing hippocampal neurons, while one control case (age, 57 years) showed extensive NFT formation, despite the absence of clinically apparent neurological deficits.

Frozen sections (20 µm) of Formalin-fixed Sommer's sector (H<sub>1</sub> region) of the hippocampus were mounted onto pure carbon disks and were viewed by scanning electron microscopy (JEOL JSM-35). Under standardized conditions of magnification, accelerating voltage (15 kV), and beam current ( $0.5 \times 10^{-10}$  Å), four sites (each measuring 0.5 µm in diameter) in the nuclear region and four in the perikaryal cytoplasm of each of ten neurons were selected for elemental analysis by energy-dispersive x-ray spectrometry (Kevex 7000 series). Emitted x-rays from each probe site were collected for 100 seconds, and the resultant x-ray energy spectra were evaluated for the presence of peaks related to the Kα x-ray emissions of magnesium, aluminum, silicon, calcium, manganese, and iron. In addition, the number of x-ray counts after background subtraction were recorded within a 150-eV window centered on the Kα of each of these elements.

Serial sections adjacent to the section used for x-ray analysis were stained by the Bielschowski silver impregnation method in order to verify the distribution and extent of NFT involvement. Since 95 percent or more of identifiable Sommer's sector neurons in affected cases contained NFT's, the need for direct confirmation of the presence of NFT's in individual neurons was unnecessary (Fig. 1). The secondary electron surface images of unstained sections provided sufficient cellular detail to identify individual neurons and landmarks for intracellular probing.

Prominent peaks related to the Kα of aluminum were found in 57.5 to 67.5

Table 1. Aluminum-related x-ray emissions (counts above background) from neurofibrillary tangle (NFT)-bearing and normal-appearing neurons of the Sommer's sector of the hippocampus in Guamanian Chamorros with amyotrophic lateral sclerosis (ALS) and parkinsonism-dementia (PD) and in neurologically normal controls.

Diagnosis	Age (years)	Sex	NFT's in hippocampus	Probe sites positive for aluminum (%)		Aluminum counts (mean ± S.E.)
				Nucleus	Cytoplasm	
ALS	64	M	4+	67.5	50.0	296.3 ± 26.2*†
PD	56	M	4+	62.5	55.0	236.2 ± 21.3*
PD	66	M	4+	57.5	52.5	232.1 ± 23.9*
Control (with NFT's)	57	M	3+	40.0	31.3	165.4 ± 13.2*
Control (without NFT's)	48	M	0	10.6	10.1	77.3 ± 7.2
	48	F				
	57	F				
	65	M				

\* $P \leq .001$  compared to control cases without NFT's (12). † $P < .01$  compared to the control case with NFT's (12).